


Spatial concentration and distribution of phase singularities in human atrial fibrillation: Insights for the AF mechanism

Madeline Schopp BEng, (Hons)¹  | Dhani Dharmapranani BEng, (Hons), PhD^{1,2} | Pawel Kuklik PhD³ | Jing Quah MBBS^{2,4} | Anandaroop Lahiri MBBS⁴ | Kathryn Tiver MBBS^{2,4} | Christian Meyer MD³ | Stephan Willems PhD³ | Andrew D. McGavigan MD⁴ | Anand N. Ganesan MBBS, PhD^{2,4}

¹College of Science and Engineering, Flinders University of South Australia, Adelaide, SA, Australia

²College of Medicine and Public Health, Flinders University of South Australia, Adelaide, SA, Australia

³Department of Cardiology, University Medical Centre, Hamburg, Germany

⁴Department of Cardiovascular Medicine, Flinders Medical Centre, Adelaide, SA, Australia

Correspondence

Anand Ganesan, College of Medicine and Public Health, Flinders University, Flinders Drive, Bedford Park, SA 5042, Australia.
Email: anand.ganesan@flinders.edu.au

Funding information

National Heart Foundation of Australia, Grant/Award Number: 101188; National Health and Medical Research Council of Australia Project Grant, Grant/Award Number: 1063754

Abstract

Background: Atrial fibrillation (AF) is characterized by the repetitive regeneration of unstable rotational events, the pivot of which are known as phase singularities (PSs). The spatial concentration and distribution of PSs have not been systematically investigated using quantitative statistical approaches.

Objectives: We utilized a geospatial statistical approach to determine the presence of local spatial concentration and global clustering of PSs in biatrial human AF recordings.

Methods: 64-electrode conventional basket (~5 min, n = 18 patients, persistent AF) recordings were studied. Phase maps were produced using a Hilbert-transform based approach. PSs were characterized spatially using the following approaches: (i) local "hotspots" of high phase singularity (PS) concentration using Getis-Ord G_i^* ($Z \geq 1.96$, $P \leq .05$) and (ii) global spatial clustering using Moran's I (inverse distance matrix).

Results: Episodes of AF were analyzed from basket catheter recordings (H: 41 epochs, 120 000 s, n = 18 patients). The Getis-Ord G_i^* statistic showed local PS hotspots in 12/41 basket recordings. As a metric of spatial clustering, Moran's I showed an overall mean of 0.033 (95% CI: 0.0003-0.065), consistent with the notion of complete spatial randomness.

Conclusion: Using a systematic, quantitative geospatial statistical approach, evidence for the existence of spatial concentrations ("hotspots") of PSs were detectable in human AF, along with evidence of spatial clustering. Geospatial statistical approaches offer a new approach to map and ablate PS clusters using substrate-based approaches.

KEYWORDS

atrial fibrillation, geospatial, mapping, phase singularity

Abbreviations: AF, atrial fibrillation; EGM, electrogram; PS, phase singularity; PSs, phase singularities.

This is an open access article under the terms of the Creative Commons Attribution-NonCommercial-NoDerivs License, which permits use and distribution in any medium, provided the original work is properly cited, the use is non-commercial and no modifications or adaptations are made.

© 2021 The Authors. *Journal of Arrhythmia* published by John Wiley & Sons Australia, Ltd on behalf of Japanese Heart Rhythm Society

1 | INTRODUCTION

Atrial fibrillation (AF) is characterized by irregular, disorganized electrical activation of the atrium.¹ A defining characteristic of AF is the presence of unstable local re-entrant circuits that form and re-form continuously during ongoing fibrillation.² The pivot of such re-entrant circuits is known as the phase singularity (PS).

In the past decade, there has been sustained interest in the possibility of mapping rotational activity as potential drivers of AF, and although initially promising, clinical findings have been difficult to uniformly reproduce.^{3–5} A key challenge is that in many studies, rotational events have been found to be temporally unstable,^{6–8} which has constrained the ability to reproducibly ablate rotational drivers.^{3,4}

Recently, there has been emerging interest in the notion that even if temporally unstable, rotational events may preferentially recur in the spatial context of critical substrates within the atrium, under the hypothesis that AF may be driven by intra-mural drivers attached to specific regions of microscopic scar within the atria.^{9–14} An attractive potential corollary of this concept is that these critical regions of substrate could possibly be identified and therefore targeted therapeutically to modify clinical outcomes.^{13,14}

To date, the spatial distribution of transient rotational events within the atrium has been studied using qualitative approaches to understand potential localization.^{6,8,10,15} We reasoned that the use of quantitative methods to identify concentrations of PS formation would have the potential to augment substrate-based ablation approaches by detecting areas with higher-than-normal PS spatial concentrations. As such, in this study, we sought to test the hypothesis that quantitative approaches from geospatial statistics could potentially identify areas of PS concentration and clustering patterns in human persistent AF.

Geospatial statistical methods have been applied to identify spatial concentration and clustering patterns in a range of disciplines including geography,¹⁶ political science,¹⁷ economics,¹⁸ and criminology.¹⁹ We hypothesized that a similar approach would identify hotspot formation and clustering of PS formation in human AF. Furthermore, utilization of a quantitative statistical approach to determine spatial associations could (i) provide an objective measure, avoiding potential heuristic bias associated with qualitative evaluation; (ii) provide a quantitative hierarchy of sites of interest; that (iii) be incorporated into automated hotspot and cluster analysis.

2 | METHODS

2.1 | Data acquisition

2.1.1 | Human AF recordings

Basket data

This study utilized a combined cohort from Flinders University and Hamburg University.²⁰ All data were obtained with written informed

consent, with study approval provided by local human ethics committees. Patients underwent biatrial mapping using 64-electrode basket catheters (Constellation, Boston Scientific, MA, 48 mm [4-mm spacing], 60 mm [5-mm spacing]) based on pre-procedural computed tomographic scans of atrial dimensions. Unipolar electrograms were recorded at a sampling frequency of 2000 kHz in induced or spontaneous AF for at least 5 min. Five-minute recordings were taken in the anterior left atrium (LA), posterior LA, and right atrium (RA). Anatomical stability was verified by regular fluoroscopic visualization and in Velocity (Abbott, IL, USA). Signals were filtered from 0.5 to 500 Hz with a sampling rate of 1000 Hz.

2.2 | Signal processing

2.2.1 | Phase calculation

All signal processing was conducted in MATLAB (version 9.3, Mathworks Inc, Natick, MA, USA). Unipolar electrograms underwent signal pre-processing filtered with 5- to 15-Hz third-order Butterworth band pass filters and 2.5- to 30-Hz third-order Butterworth band pass filters. Signals underwent QRS subtraction.²¹ Sinusoidal recomposition was performed.²² Phase reconstruction was performed using the Hilbert transform.²³ PS detection and tracking were performed using previously described methods.^{7,24}

2.3 | Geospatial analysis

2.3.1 | Getis-Ord G_i^* as a measure of spatial concentration for hotspot and cold spot analysis

To check for the local concentrations of low or high phase singularities (PSs) (cold spot and hotspot analysis), the Getis-Ord G_i^* ²⁵ statistic was used. The Getis-Ord G_i^* statistic works to detect the presence of local hotspots and cold spots in a dataset. A hotspot is a spatial region with a statistically significant higher standardized z-score than immediately surrounding areas for the variable of interest. A cold spot is a spatial region with a statistically significant lower standardized z-score than immediately surrounding areas for the variable of interest.

For this study, the resultant z-score identified locations as having high or low values of PSs spatially by comparing each feature in the dataset with neighboring features. Locations were defined as physical electrodes in the anatomic map. To be considered a hot or cold spot, statistically significant z-scores needed to be surrounded by other statistically significant z-scores.

To calculate the G_i^* statistic, the following formula was implemented:

$$G_i^* = \frac{\sum_{j=1}^n w_{ij} x_j - \bar{X} w_{ij}}{s \sqrt{\frac{n \sum_{j=1}^n w_{ij}^2 - (\sum_{j=1}^n w_{ij})^2}{n-1}}} \quad (1)$$

Here, $\bar{X} = \frac{\sum_{j=1}^n x_j}{n}$, $S = \sqrt{\frac{\sum_{j=1}^n x_j^2}{n} - (\bar{X})^2}$ and x_j represented the attribute value for the element j . Since the G_i^* statistic is a z-score, no further calculations were required. A schematic showing Getis-Ord G_i^* is shown in Figure 1.

2.3.2 | Moran's I

To examine spatial clustering, we used Moran's I ,²⁶ which is a measure of spatial autocorrelation. Spatial autocorrelation is an important parameter describing the degree of similarity between values of a given variable in one location and its surrounding neighbors.²⁷ Positive spatial autocorrelation occurs when neighboring values tend to have similar values (ie, clustering of like values), whereas negative spatial autocorrelation arises when neighboring values have dissimilar values.²⁸

Specifically, the concept of spatial clustering is the process of grouping objects into classes called clusters such that objects within a cluster have high similarity to one another but are dissimilar to objects in other clusters.²⁹ Moran's I can distinguish three major types of patterns in spatial distribution: (i) spatially clumped or clustered data, (ii) uniformly distributed data, and (iii) randomly distributed data (Figure 2). Moran's I ranges between negative one and positive one depending on the degree of spatial autocorrelation observed globally. A schematic illustrating this can be seen in Figure 2.

Moran's I is a correlation coefficient measuring the global covariance of values in a dataset:

$$I = \frac{n}{\sum_i \sum_j w_{ij}} \frac{\sum_i \sum_j w_{ij} (x_i - \bar{X})(x_j - \bar{X})}{\sum_i (x_i - \bar{X})^2} \quad (2)$$

Here, n was defined as the number of spatial features x_p , $i = 1, 2, \dots, N$, while \bar{X} represents the mean of x_p , where $x_i - \bar{X}$ is the deviation of an attribute for feature i from its mean. w_{ij} is a spatial weights matrix.

2.3.3 | Spatial weights matrix

Calculation of Moran's I relies on a measure of the configuration of the spatial units being studied, often referred to as a spatial weights matrix (w_{ij}).²⁷ Spatial weights matrices represent the spatial weight between feature i and feature j , recording the spatial association among spatial units being studied.³⁰ In order to assess the presence of global clustering of like values in PS formation, we calculated Moran's I using the inverse distance weights matrix. The inverse distance weights matrix was constructed based on the following equation:

$$w_{ij} = \begin{cases} d_{ij}^{-\alpha} & \text{if } i \neq j \\ 0 & \text{if } i = j \end{cases} \quad (3)$$

where $\alpha = 1$ and d_{ij} represented the anatomical distance between region i and j . Shortest anatomical distances between electrodes were computed using Dijkstra's shortest path algorithm.³¹ Row standardization was performed on the spatial weights matrix model to remove dependence on extraneous scale factors.

2.4 | Statistical analysis

Computational analysis of Getis Ord G_i^* and Moran's I were conducted in custom MATLAB software. Results are expressed as mean \pm SD unless otherwise stated. Statistical analysis of data was performed using SPSS, with $z \geq 1.96$ and $P \leq .05$ considered statistically significant.

3 | RESULTS

A total of 41 epochs from 18 patient recordings were analyzed. The baseline characteristics of the study population are as follows: age 62 (95% CI: 58, 65), 15/18 male (83%), 18/18 persistent AF (100%), BMI 28.9 (95% CI: 26.5, 31.1), LVEF 58.0% (95% CI: 54.2, 61.7%), LA diameter 44.0 mm (95% CI: 41.0, 47.2), and CHA₂DS₂-VASc 1.3 (95% CI: 0.8, 1.9).

3.1 | Spatial concentration of PSs

Using Getis-Ord G_i^* , we identified areas with significant spatial concentration in 29.3% (12/41) of epochs. Example maps showing hot and cold spots are shown in Figure 3. Areas of high or low spatial concentration were considered to be statistically significant when a group of statistically significant z-scores ($z \geq 1.96$ or $z \leq -1.96$) was surrounded by other statistically significant z-scores.

We found hotspots (areas of high local spatial concentration of PSs) in 22.0% (9/41) of basket catheter recordings. In total, 10 hotspots were identified—four in the LA and six in the RA. The majority of hotspots (9/10) occurred as unique areas of high spatial PS concentration for individual epochs, with only one recording demonstrating the simultaneous presence of two hotspots. The average size of the hotspot cluster was found to be 3.5 nodes (95% CI: 2.359-4.641).

Cold spots (areas of low spatial concentration) were identified in 19.5% (8/41) of basket catheter recordings. A total of nine cold spots were detected—two in the LA and seven in the RA. In the case of cold spots, again the majority (8/9) were detected as unique areas of low PS concentration for the individual epoch concerned, with only one recording showing the presence of two simultaneous cold spots. The average size of a cold spot cluster was found to be 2.8 (95% CI: 2.064-3.492) nodes. Five epochs were found to have both a hotspot and a cold spot.

3.2 | Spatial distribution PS formation using Moran's *I*

Moran's *I* was utilized to identify evidence of clustering of PS formation in human persistent AF. Figure 4 shows example grid maps of the global clustering patterns observed using Moran's *I*. We split the calculated Moran's *I* values into three groups so that conclusions could be drawn regarding the observed clustering. Groups were separated as (i) those with positive values of Moran's *I* and $P < .05$ indicating spatial clustering or clumping (as in Figure 2A), (ii) those with positive Moran's *I* near to zero and $P > .05$ suggesting complete spatial randomness (as in Figure 2B), and (iii) those with negative values of Moran's *I* close to 0 and $P > .05$ showing complete spatial randomness (as in Figure 2B).

17.1% (7/41) of epochs from basket catheter recording were found to align with the first group of Moran's *I* values, producing positive and statistically significant values of Moran's *I* and therefore

indicating some form of spatial clustering or clumping. About 28.6% (2/7) of this spatial clustering was observed in the LA, and 71.4% (5/7) was observed in the RA. Figure 4A shows example cases of the statistically significant Moran's *I* grid maps of PS formation. In this group, since the magnitude of Moran's *I* was found to be < 0.25 , it is suggested that PS clustering was modest (mean Moran's *I* = 0.1678, 95% CI: 0.1077-0.2280).

82.9% (34/41) of epochs were found to be non-statistically significant and, therefore, indicate complete spatial randomness. About 51.2% (21/41) were found to align with group (ii), having positive values of Moran's *I*, with $P > 0.05$ (mean Moran's *I* 0.0583, 95% CI: 0.0143-0.0651). Examples of these cases can be seen in Figure 4B. The remaining 31.7% (13/41) of epochs were found to have negative values of Moran's *I* and align best with group (iii). All of these epochs showed $P > 0.05$ and were close to 0, most consistent with complete spatial randomness of PS formation (-0.0817 , 95% CI: -0.1435 to -0.0208). Example cases of negative values of Moran's *I* can be seen in Figure 4C.

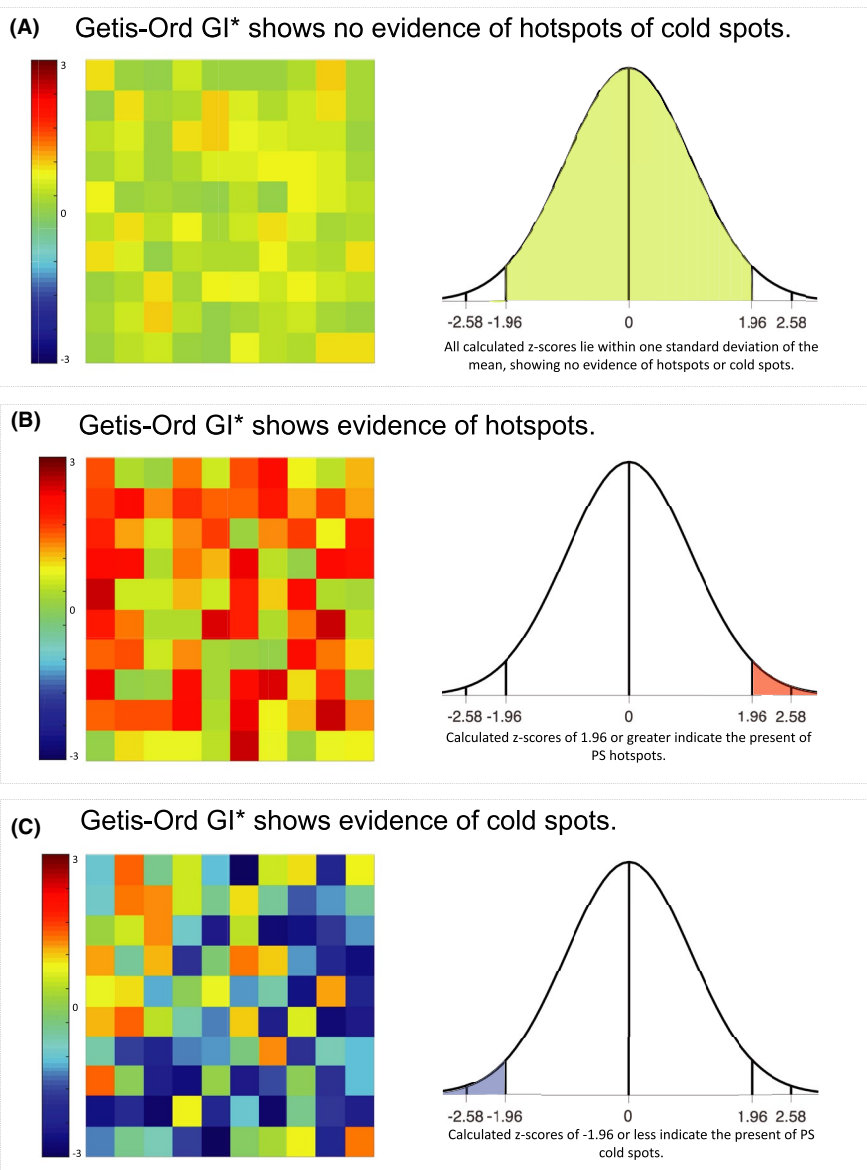


FIGURE 1 Getis-Ord G_i^* Detects High and Low Spatial Concentrations. Examples of calculated z-scores for three quantitatively different scenarios of spatial concentration. Statistically significant ($z \geq 1.96$ or $z \leq -1.96$) spatial hotspots and cold spots are identified. (A) Getis-Ord G_i^* shows no evidence of hotspots or cold spots, with all calculated z-scores being statistically insignificant ($-1.96 \leq z \leq 1.96$). (B) Getis-Ord G_i^* shows evidence of hotspots, with z-scores falling in the statistically significant range ($z \geq 1.96$). (C) Getis-Ord G_i^* shows evidence of cold spots, with z-scores falling in the statistically significant range ($z \leq -1.96$)

Figure 5 shows a box and whisker plot for Moran's I across the basket catheter recordings. For basket recordings, over both the LA and RA, Moran's I was found to range between -0.2050 and 0.2885 and, on average, was calculated to be 0.0326 (95% CI: 0.0003 - 0.0649). Considering Moran's I values in the LA, the average was found to be 0.0252 (95% CI: -0.0375 to 0.0898). In the RA, where the mean was 0.0485 (95% CI: -0.0187 to 0.1157). The proximity to zero, in conjunction with the absence of statistical significance of Moran's I values, is consistent with the notion that PSs are randomly dispersed through the atrium.

4 | DISCUSSION

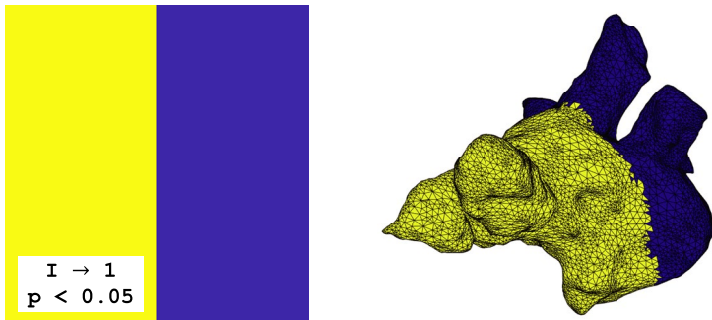
In this study, we sought to investigate and understand the spatial concentration of PSs using statistical approaches adapted from geospatial science. Here, we quantitatively investigated the spatial distribution of PS formation in human persistent AF. The principal finding

of our study was that when using conventional electrogram-based basket mapping techniques, PSs appear to form in concentrated hot-spots and cold spots within the atrium. We found limited evidence to suggest spatial clustering of PSs across the entire atria, with results indicating that overall, PSs are randomly dispersed throughout the atrium. These results may be of clinical significance in the mapping of critical substrates in AF, where areas of high or low concentrations of PSs may form targetable areas for AF ablation therapy.

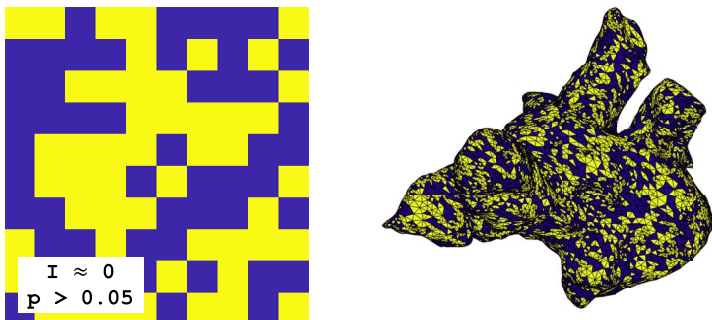
4.1 | Unstable fibrosis linked rotors: A new conceptual paradigm

The notion of unstable fibrosis-linked rotors has recently entered the field of understanding of contemporary AF mechanisms. Under this theory, driving re-entrant circuits could potentially be anchored to critical areas of micro-substrate, created by localized

(A) Moran's I demonstrates clear evidence of spatial clustering.



(B) Moran's I demonstrates complete spatial randomness.



(C) Moran's I demonstrates uniform spatial dispersion.

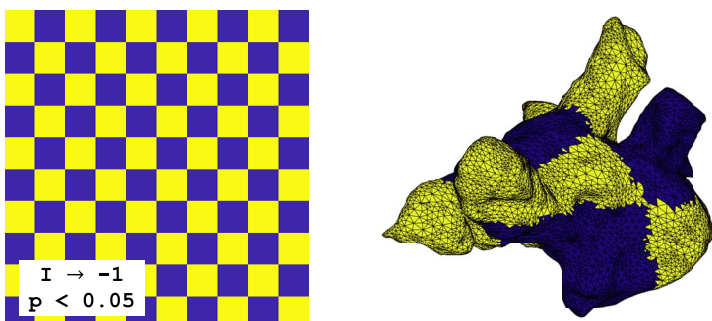


FIGURE 2 Moran's I detects spatial autocorrelation. Examples of spatial patterns for three quantitatively different scenarios of Moran's I . Each cell value is either 0 (blue) or 1 (yellow). (A) Moran's I demonstrates clear spatial clustering or clumping. In this scenario, I approaches 1, and P -values are significant, reflecting the homogeneity between states of neighbouring cells. (B) Moran's I demonstrates spatial randomness. In this scenario, I values are close to 0, with $P > .05$, reflecting the randomness of the pattern observed. (C) Moran's I demonstrates a uniform spatial dispersion. In this scenario, neighboring cells have opposing values at all four borders, resulting, I values near to -1 , and $P < .05$

FIGURE 3 Getis-Ord G_i^* analysis shows evidence of PS hotspots. Getis-Ord G_i^* analysis was performed to identify statistically significant ($z \geq 1.96$ or $z \leq -1.96$) spatial hotspots and cold spots of PS formation. (A) Basket catheter grid maps show evidence of localized areas of high concentration of PS formation, indicating the presence of a hotspot. (B) Basket catheter grid maps show evidence of localized areas of low concentration of PS formation, indicating the presence of a cold spot. (C) Basket catheter grid maps show evidence of localized areas of both high concentration of PS formation and low concentration of PS formation, indicating the presence of hotspots and cold spots in a single recording

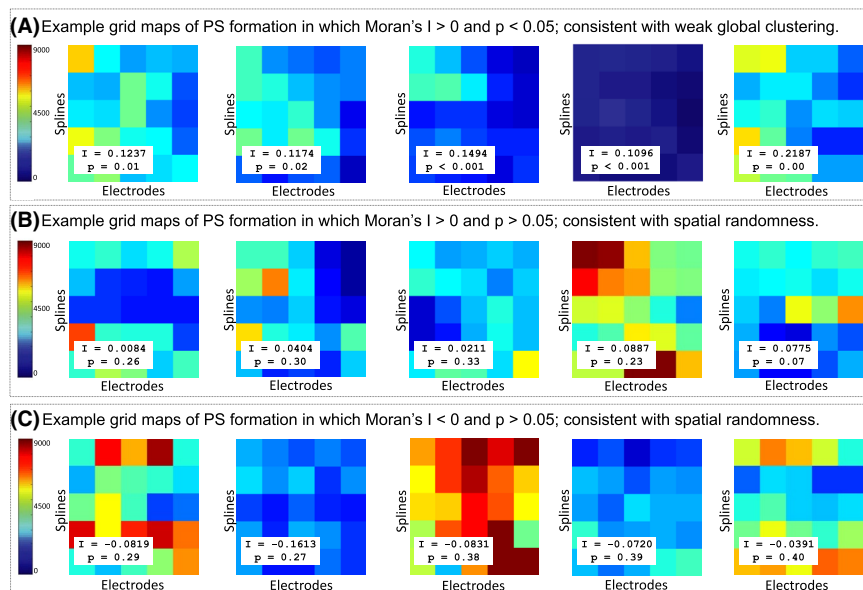
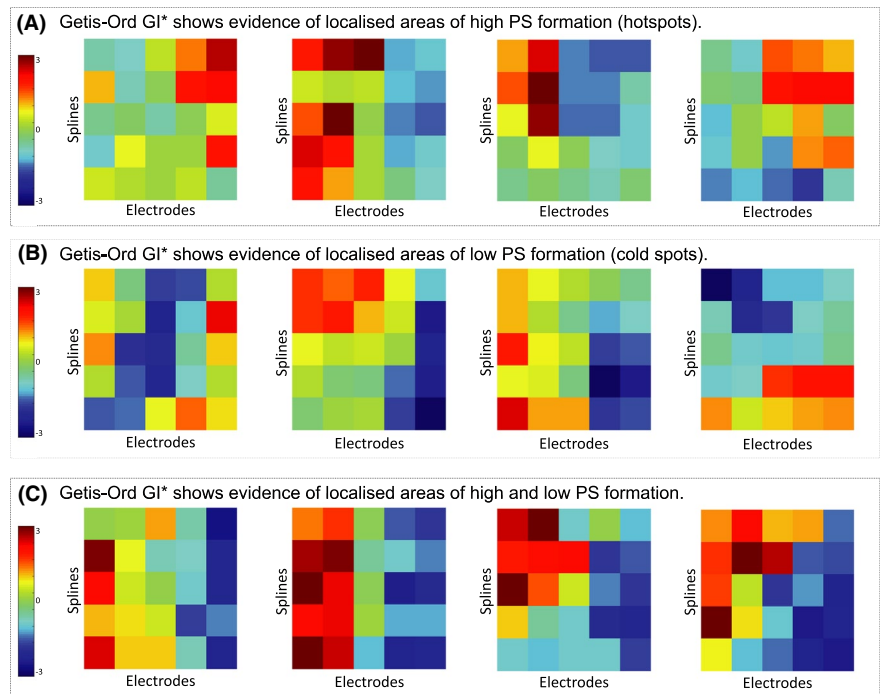


FIGURE 4 Global clustering of phase singularity formation. Examples of basket catheter grid maps of PS formation in human persistent AF. (A) Grid maps of PS formation for positive values of Moran's I showing statistical significance, thus indicating modest spatial clustering or clumping. (B) Grid maps of PS formation for positive values approaching zero of Moran's I showing no statistical significance; thus consistent with complete spatial randomness. (C) Grid maps of PS formation for negative values of Moran's I near to zero, showing no statistical significance; thus, consistent with spatial randomness. Overall, Moran's I is consistent with the notion that PSs are randomly dispersed through the atrium in human persistent AF

scar.^{9,10,12,13,32} According to this hypothesis, AF could be maintained by critical areas of substrate that could act as fixed locations for unstable re-entrant circuits to form around, providing a reconciling mechanism that could allow for the observed temporal instability of rotors,⁹ but support the notion that critical substrate areas could be targeted to modulate the atrium's propensity to support AF. Emerging evidence has suggested key substrates identified through a combination of imaging-guided mapping in

combination with computational modelling may lead to acute impact on AF dynamics.^{10,32-34}

4.2 | Ablation of rotors in human persistent AF

Unstable re-entrant circuits known as rotors are a defining feature of cardiac fibrillation, first identified over a century ago.³⁵ Over the past

Moran's I shows evidence of spatial randomness of PS formation in a majority of cases.



FIGURE 5 Clustering of phase singularity formation using Moran's *I*. Moran's *I* shows evidence of spatial randomness of PS formation for a majority of cases. Overall, the Moran's *I* statistic showed a mean of 0.0326 (95% CI: 0.0003-0.0649). In the LA, the mean Moran's *I* was found to be 0.0252 (95% CI: -0.0375 to 0.0898) and in the RA the mean Moran's *I* was 0.0485 (95% CI: -0.0187 to 0.1157)

few decades, the role of these circuits as potential drivers of AF has been demonstrated in multiple pre-clinical investigations.³⁶⁻³⁸ This has led to growing interest in the idea that rotor behavior could be directly targeted by catheter ablation,^{39,40} resulting in termination of AF and potentially improved clinical outcomes. Unfortunately, clinical outcomes of these studies have not been uniform,^{3,4,41} leading to a search for potential alternative approaches based on driver-based ablation.

4.3 | Reconciling the spatial concentration of re-entrant circuits with PS renewal

Early investigations of the localization of rotors with critical substrate have predominantly adopted a qualitative approach to evaluate this spatial association.^{10,34} Qualitative approaches, however, may have the potential to introduce heuristic bias.^{42,43} As such, we sought to test the hypothesis that quantitative approaches from geospatial statistics could potentially identify PS formation clusters in human persistent AF, an approach well validated in other scientific and social science discipline.¹⁶⁻¹⁹

An important concept that was clear from the current data is that the relative number of PS hotspots in the atrium was relatively small in comparison to the dynamic renewal of unstable PSs that is typically observed in AF.²⁴ This discrepancy could be reconciled by considering that PS formation most likely occurs as a consequence of tissue micro-structural heterogeneities in combination with dynamic functional factors.⁴⁴ According to this idea, areas of local hotspot concentration could be hypothesized to be occurring via the

effect of relatively fixed heterogeneities in the myocardium caused by areas of micro-fibrosis.⁴⁵ On the other hand, many and perhaps, most, PSs occur as a consequence of dynamic alterations in tissue conduction and refractoriness.

The data supports a conceptualization of AF maintenance occurring via the interplay of structural substrate related renewal of PSs in combination with dynamic PS regeneration. This could account for the observation that PS formation and destruction at the global level converge to stable rates that are able to be determined by modelling PS creation and annihilation and Poisson renewal processes.²⁴ The fact that both tissue and physiological factors are likely to be important to sustaining AF may become clinically relevant in understanding the progression of AF from paroxysmal to persistent as well as determining the likelihood of clinical response to AF ablation. We are currently conducting a prospective clinical study, RENEWAL AF, to explore these questions.⁴⁶

4.4 | Clinical implications

Our study has implications for contemporary efforts to ablate drivers in AF. If a strategy of focal driver ablation is considered, then a geospatial statistical approach may be beneficial as it is quantitative and non-biased and allows for objective identification of hotspots, cold spots, and PS clustering, which may highlight mechanistically important areas of the atrium. The identification of these areas of high PS concentration may also help to target ablation therapies and may assist in the validation of, and be additive to, substrate or imaging guided approaches which are currently under evaluation in AF ablation.

4.5 | Study limitations

Conventional basket catheters are known to have limitations in terms of their anatomical contact and spatial resolution with the endocardial surface of the atrium. The absence of clustering observed in this study may reflect the relatively low resolution of contemporary basket catheters. A specific area that current baskets are not able to address is to simultaneously map the pulmonary veins, appendages, and body of the atria with adequate spatial resolution. As such, we were not able to specifically measure PS concentrations in the basket catheter and could not draw conclusions regarding the concentration of PSs in the pulmonary veins. Improvements in mapping catheter design and technology may in future be able to address this gap.⁴⁶

An issue that is not fully resolved is whether basket-type catheters may be effective in the mapping of PSs. While in general, it has been suggested that basket catheters may have the theoretical risk of false detection of PSs, we have recently shown that rate constants of PS formation and destruction detected by basket catheters can accurately predict the number and population distribution of observed PS, in line with a property of scale invariance under transformation.⁴⁷ This issue would therefore be considered as under debate in the literature at the current time.

A further limitation of the current retrospective study design was that the relationship to clinical arrhythmia outcomes could not be addressed. No ablation was performed on regions of PS concentration, so we were unable to confirm whether these regions were mechanistically significant in sustaining AF. As the intention of this study, however, was to evaluate the mechanistic feasibility of using a geospatial statistical approach to identify areas of PS concentration and clustering, improvements in catheter mapping technologies such as the development of anatomically conformant catheters may in future address the contemporary hardware limitations of current basket catheter technology.

The study also had some important limitations in terms of the technical approach used for PS detection. The double-ring PS detection approach adopted in this study has the effect of reducing the area available for PS detection. This could potentially decrease the sensitivity for hotspot detection, but those hotspots that were detected were most likely to be valid. A further limitation of the study is that the temporal stability of the hotspots detected was not able to be assessed beyond the 5-min detection window. Further investigation into the temporal stability of hotspots is therefore warranted to determine if these locations are spatiotemporally stable over time.

In addition, in this study, the lack of scar imaging by CMR meant that we were unable to investigate whether or not a correlation between scar and areas of high or low PS concentration exists. Further studies are required to assess the impact of these regions in PS concentration and clustering.

5 | CONCLUSION

Using a systematic, quantitative geospatial statistical approach, evidence of spatial concentration of PS formation was observed in human atrial fibrillation, along with evidence of spatial clustering.

Further investigations are required to determine if these approaches may be of significance to current efforts to map and ablate phase singularities using substrate-based approaches.

ACKNOWLEDGEMENTS

This work was supported by the National Health and Medical Research Council of Australia Project Grant (1063754) and National Heart Foundation of Australia (101188).

CONFLICTS OF INTEREST

Authors declare no conflict of interests for this article.

ORCID

Madeline Schopp  <https://orcid.org/0000-0002-3029-2329>

REFERENCES

- Schotten U, Verheule S, Kirchhof P, Goette A. Pathophysiological mechanisms of atrial fibrillation: a translational appraisal. *Physiol Rev*. 2011;91(1):265–325.
- Nattel S, Xiong F, Aguilar M. Demystifying rotors and their place in clinical translation of atrial fibrillation mechanisms. *Nat Rev Cardiol*. 2017;14(9):509–20.
- Benharash P, Buch E, Frank P, Share M, Tung R, Shivkumar K, et al. Quantitative analysis of localized sources identified by focal impulse and rotor modulation mapping in atrial fibrillation. *Circ Arrhythm Electrophysiol*. 2015;8(3):554–61.
- Steinberg JS, Shah Y, Bhatt A, Sichrovsky T, Arshad A, Hansinger E, et al. Focal impulse and rotor modulation: acute procedural observations and extended clinical follow-up. *Heart Rhythm*. 2017;14(2):192–7.
- Parameswaran R, Voskoboinik A, Gorelik A, Lee G, Kistler PM, Sanders P, et al. Clinical impact of rotor ablation in atrial fibrillation: a systematic review. *Europace*. 2018;20(7):1099–106.
- Pathik B, Kalman JM, Walters T, Kuklik P, Zhao J, Madry A, et al. Transient rotor activity during prolonged 3-dimensional phase mapping in human persistent atrial fibrillation. *JACC Clin Electrophysiol*. 2018;4(1):72–83.
- Kuklik P, Zeemering S, van Hunnik A, Maesen B, Pison L, Lau DH, et al. Identification of rotors during human atrial fibrillation using contact mapping and phase singularity detection: technical considerations. *IEEE Trans Biomed Eng*. 2017;64(2):310–8.
- Child N, Clayton RH, Roney CR, Laughner JI, Shuros A, Neuzil P, et al. Unraveling the underlying arrhythmia mechanism in persistent atrial fibrillation: results from the STARLIGHT study. *Circ Arrhythm Electrophysiol*. 2018;11(6):e005897.
- Csepe TA, Hansen BJ, Fedorov VV. Atrial fibrillation driver mechanisms: insight from the isolated human heart. *Trends Cardiovasc Med*. 2017;27(1):1–11.
- Hansen BJ, Zhao J, Csepe TA, Moore BT, Li N, Jayne LA, et al. Atrial fibrillation driven by micro-anatomic intramural re-entry revealed by simultaneous sub-epicardial and sub-endocardial optical mapping in explanted human hearts. *Eur Heart J*. 2015;36(35):2390–401.
- Zhao J, Hansen BJ, Wang Y, Csepe TA, Sul LV, Tang A, et al. Three-dimensional integrated functional, structural, and computational mapping to define the structural “fingerprints” of heart-specific atrial fibrillation drivers in human heart ex vivo. *J Am Heart Assoc*. 2017;6(8).
- Haissaguerre M, Shah AJ, Cochet H, Hocini M, Dubois R, Efimov I, et al. Intermittent drivers anchoring to structural heterogeneities as a major pathophysiological mechanism of human persistent atrial fibrillation. *J Physiol*. 2016;594(9):2387–98.

13. Boyle PM, Hakim JB, Zahid S, Franceschi WH, Murphy MJ, Prakosa A, et al. The fibrotic substrate in persistent atrial fibrillation patients: comparison between predictions from computational modeling and measurements from focal impulse and rotor mapping. *Front Physiol.* 2018;9:1151.
14. Boyle PM, Hakim JB, Zahid S, Franceschi WH, Murphy MJ, Vigmond EJ, et al. Comparing reentrant drivers predicted by image-based computational modeling and mapped by electrocardiographic imaging in persistent atrial fibrillation. *Front Physiol.* 2018;9:414.
15. Pathik B, Kalman JM, Walters T, Kuklik P, Zhao J, Madry A, et al. Absence of rotational activity detected using 2-dimensional phase mapping in the corresponding 3-dimensional phase maps in human persistent atrial fibrillation. *Heart Rhythm.* 2018;15(2):182–92.
16. Anselin L. Local indicators of spatial association—LISA. *Geographical analysis.* 1995;27(2):93–115.
17. O'Loughlin J. Spatial analysis in political geography. A companion to political geography. 2003(Feb):30–46.
18. Anselin L. *Spatial econometrics: Methods and models.* Springer Science & Business Media; 2013.
19. Baller RD, Anselin L, Messner SF, Deane G, Hawkins DF. Structural covariates of US county homicide rates: incorporating spatial effects. *Criminology.* 2001;39(3):561–88.
20. Dharmapran D, McGavigan AD, Chapman D, Kutlieh R, Thanigaimani S, Dykes L, et al. Temporal stability and specificity of high bipolar electrogram entropy regions in sustained atrial fibrillation. *J Electrocardiol.* 2019;53:18–27.
21. Shkurovich S, Sahakian AV, Swiryn S. Detection of atrial activity from high-voltage leads of implantable ventricular defibrillators using a cancellation technique. *IEEE Trans Biomed Eng.* 1998;45(2):229–34.
22. Kuklik P, Zeemering S, Maesen B, Maessen J, Crijns HJ, Verheule S, et al. Reconstruction of instantaneous phase of unipolar atrial contact electrogram using a concept of sinusoidal recomposition and Hilbert transform. *IEEE Trans Biomed Eng.* 2015;62(1):296–302.
23. Nash MP, Mourad A, Clayton RH, Sutton PM, Bradley CP, Hayward M, et al. Evidence for multiple mechanisms in human ventricular fibrillation. *Circulation.* 2006;114(6):536–42.
24. Dharmapran D, Schopp M, Kuklik P, Chapman D, Lahiri A, Dykes L, et al. Renewal Theory as a universal quantitative framework to characterize phase singularity regeneration in mammalian cardiac fibrillation. *Circ Arrhythm Electrophysiol.* 2019;12(12):e007569.
25. Getis A, Ord JK. The analysis of spatial association by use of distance statistics. *Geographical Analysis.* 1992;24(3):189–206.
26. Moran PA. The interpretation of statistical maps. *J R Stat Soc Ser B (Methodol).* 1948;10(2):243–51.
27. Getis A. Reflections on spatial autocorrelation. *Reg Sci Urban Econ.* 2007;37(4):491–6.
28. Schmal C, Myung J, Herzel H, Bordyugov G. Moran's I quantifies spatio-temporal pattern formation in neural imaging data. *Bioinformatics.* 2017;33(19):3072–9.
29. Han J, Kamber M, Tung AK. Spatial clustering methods in data mining. *Geographic data mining and knowledge discovery.* 2001:188–217.
30. Getis A. Spatial autocorrelation. In: Fischer MM, Getis A, editors. *Handbook of applied spatial analysis: Software tools, methods and applications.* Berlin, Heidelberg: Springer Berlin Heidelberg; 2010. p. 255–78.
31. Dijkstra EW. A note on two problems in connexion with graphs. *Numer Math.* 1959;1(1):269–71.
32. Hansen BJ, Zhao J, Fedorov VV. Fibrosis and atrial fibrillation: computerized and optical mapping; a view into the human atria at submillimeter resolution. *JACC Clin Electrophysiol.* 2017;3(6):531–46.
33. Boyle PM, Zghaib T, Zahid S, Ali RL, Deng D, Franceschi WH, et al. Computationally guided personalized targeted ablation of persistent atrial fibrillation. *Nat Biomed Eng.* 2019;3:870–9.
34. Li N, Csepe TA, Hansen BJ, Sul LV, Kalyanasundaram A, Zakharkin SO, et al. Adenosine-induced atrial fibrillation: localized reentrant drivers in lateral right atria due to heterogeneous expression of adenosine A1 receptors and GIRK4 subunits in the human heart. *Circulation.* 2016;134(6):486–98.
35. Garrey WE. The nature of fibrillatory contraction of the heart: its relation to tissue mass and form. *Am J Physiol.* 1914;33:397–414.
36. Mansour M, Mandapati R, Berenfeld O, Chen J, Samie FH, Jalife J. Left-to-right gradient of atrial frequencies during acute atrial fibrillation in the isolated sheep heart. *Circulation.* 2001;103(21):2631–6.
37. Mandapati R, Skanes A, Chen J, Berenfeld O, Jalife J. Stable microreentrant sources as a mechanism of atrial fibrillation in the isolated sheep heart. *Circulation.* 2000;101(2):194–9.
38. Chen J, Mandapati R, Berenfeld O, Skanes AC, Gray RA, Jalife J. Dynamics of wavelets and their role in atrial fibrillation in the isolated sheep heart. *Cardiovasc Res.* 2000;48(2):220–32.
39. Narayan SM, Krummen DE, Shivkumar K, Clopton P, Rappel WJ, Miller JM. Treatment of atrial fibrillation by the ablation of localized sources: CONFIRM (Conventional Ablation for Atrial Fibrillation With or Without Focal Impulse and Rotor Modulation) trial. *J Am Coll Cardiol.* 2012;60(7):628–36.
40. Haissaguerre M, Hocini M, Denis A, Shah AJ, Komatsu Y, Yamashita S, et al. Driver domains in persistent atrial fibrillation. *Circulation.* 2014;130(7):530–8.
41. Brachmann J, et al. LBCT01-02. Presented at: Heart Rhythm Society Annual Scientific Sessions; May 8–11, 2019; San Francisco.
42. Todorovic D. Gestalt principles. *Scholarpedia.* 2008;3(12):5345.
43. Coren S, Girgus JS. Principles of perceptual organization and spatial distortion: the gestalt illusions. *J Exp Psychol Hum Percept Perform.* 1980;6(3):404.
44. Weiss JN, Qu Z, Chen P-S, Lin S-F, Karagueuzian HS, Hayashi H, et al. The dynamics of cardiac fibrillation. *Circulation.* 2005;112(8):1232–40.
45. Quah JX, Dharmapran D, Tiver K, Lahiri A, Hecker T, Perry R, et al. Atrial fibrosis and substrate based characterization in atrial fibrillation: time to move forwards. *J Cardiovasc Electrophysiol.* 2021;32(4):1147–60.
46. Quah J, Dharmapran D, Lahiri A, Schopp M, Mitchell L, Selvanayagam JB, et al. Prospective cross-sectional study using Poisson renewal theory to study phase singularity formation and destruction rates in atrial fibrillation (RENEWAL-AF): study design. *J Arrhythm.* 2020;36(4):660–7.
47. Dharmapran D, Jenkins E, Aguilar M, Quah JX, Lahiri A, Tiver K, et al. M/M/infinity birth-death processes—a quantitative representational framework to summarize and explain phase singularity and wavelet dynamics in atrial fibrillation. *Front Physiol.* 2021;11:616866.

How to cite this article: Schopp M, Dharmapran D, Kuklik P, et al. Spatial concentration and distribution of phase singularities in human atrial fibrillation: Insights for the AF mechanism. *J Arrhythmia.* 2021;37:922–930. <https://doi.org/10.1002/joa3.12547>